Ice-Rich Crater Fills in the Martian Mid-Latitudes: Morphology, Distribution, and Implications for Mid-Latitude Ice Stability

Hiral Bijoy, Trishit Ruj, Jun Kameda, Takaki Sako

Institute for Planetary Materials, Okayama University, Tottori 682-0193, Japan (hiralpb@s.okayama-u.ac.jp)

Introduction:

Identifying and mapping ice-rich landforms is crucial for reconstructing recent climate evolution on Mars and estimating the current volume of preserved subsurface water ice. In the Martian mid-latitudes, impact craters frequently contain infillings of dust, debris, and ice, collectively referred to as crater fills. A notable subtype, Concentric Crater Fill (CCF), is characterized by concentric, lineated deposits formed by ice-related processes and preserved on crater floors. The volume of preserved ice is highest in CCFs, making them efficient reservoirs where a large amount of ice is concentrated in a localized area with minimal energy expenditure. As a result, CCFs are considered promising targets for in-situ resource utilization (ISRU) in future human missions to Mars, offering accessible and abundant water ice.

Levy et al. (2009, 2010, 2014) broadly categorized CCF into "classic" and "low definition" types based on morphological characteristics. Previous studies have largely focused on quantifying the volume of subsurface ice, its present distribution, and its evolution under changing climate conditions.

Based on this, the present study asks a different but complementary question: Why are ice-rich crater fills preferentially distributed in specific regions? We investigate how latitude-dependent climatic gradients and crater-specific properties, such as size, depth, and age they affect their spatial distribution. To address this, we mapped and classified over 4000 impact craters (≥2 km in diameter) between 25° and 60°N, a region known for episodic water ice accumulation and widespread glacial modification.

Methods:

We analyzed 4106 impact craters (≥2 km in diameter) between 25° and 60°N using CTX (~6 m/pixel) and HiRISE (~0.3 m/pixel) images, along with MOLA topography (~200 m/pixel). Crater mapping was conducted in ArcGIS Pro, and all classifications were performed manually using morphological criteria derived from previous glacial and periglacial studies.

Crater fill classification: We identified six distinct crater fill types based on morphological characteristics and inferred ice content, reflecting a continuum of preservation and degradation. This classification scheme was developed by synthesizing previous frameworks (e.g., Levy et al., 2009) and expanded based on our own mapping to better capture intermediate and degraded fill states. Types 1 and 2 exhibit well-defined, lineated fills that fully cover the crater interior, indicating the highest present-day ice content. Type 3 shows partial infilling and subdued textures, consistent with moderate ice retention. Type 4 is characterized by eroded, wall-confined deposits, suggesting low residual ice. Type 5 displays surface features associated with advanced sublimation, implying significant past ice content but current degradation. Type 6 represents craters with evidence of former ice, now modified by periglacial and seasonal processes. This classification integrates morphology and preservation state to assess current and past ice distribution on Mars.

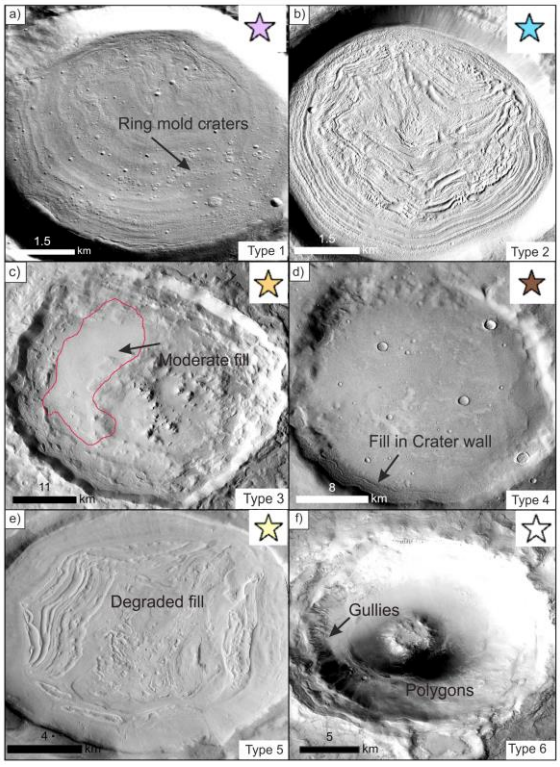

Fig 1: (a) Type 1 HDFR with multiple ring-mold craters. (b) Type 2 HDF with lineated textures and no visible ring-mold craters. (c) Type 3 MDF partially covering the crater floor with concentric features. (d) Type 4 LDF confined to crater walls. (e) Type 5 DIRF with irregular pits and chaotic textures. (f) Type 6 PF showing polygons and gullies. (colored stars indicate crater types in Fig. 2 and 3). North is pointing up in all these images.

Type 1, High-Definition Fills with Ring-Mold Craters (HDFR), are characterized by concentric ridges, flow lineations, and rimless craters with distinct central features (ring-mold craters) (Kress and Head, 2008) (Fig.1a), indicative of relatively pure near-surface ice and a thin debris cover. These morphologies suggest a near-surface ice-rich substrate and subsequent erosion as a source of fresh ice in mid-latitudinal mantles. Type 2, High-Definition Fills (HDF) display lineated textures and flow-like features but lack ring-mold craters, implying ice-rich sediments or buried massive ice with limited impact activity or surface exposure (Fig.1b). Type 3, Moderate-Definition Fills (MDF) partially cover crater floors and preserve faint concentric features, sug-

gesting partial degradation (Fig.1c). Type 4 Low-Definition Fills (LDF) are mostly confined to crater walls and show degraded glacial morphologies, reflecting greater erosion or reduced ice retention (Fig.1d). Type 5 Degraded Ice-Rich Fills (DIRF) feature irregular pits, brain terrain, and chaotic textures, indicating substantial ice loss through sublimation and collapse (Fig.1e). Finally, Type 6 paraglacial fill (PF) represents post-glacial modification, exhibiting features such as polygons (caused by seasonal contraction and expansion of shallow ground ice) and gullies formed by seasonal thermal contraction and shallow ice melting formation, collectively interpreted as surface degradation following the retreat of subsurface ice (Fig.1f).

Distributions of Crater Fills in the Northern Mid-Latitude: In the Northern Hemisphere, Type 1(0-30° E, 60-120° W) and Type 2 (0-60° E) crater fills have high content of preserved fills and are concentrated in the lower mid-latitudes (25°–40°N) due to the structure of stationary planetary waves and topographic forcing induced by the Tharsis, Arabia, and Elysium barriers. In contrast, Type 5 (40°–100°E) and Type 6 (40°–90°E) represent degraded fills, found in the upper mid-latitudes (≥35°N). Their distribution is consistent with the migration of the mid-latitude cloud belt under non-dusty conditions (Madeleine et al., 2006), where sublimation exceeds accumulation, leading to significant ice loss.

Our mapping results show that the highest present-day ice content is located between 30°–42°N, particularly within the longitudinal bands of 0°–45°E and 50°–100°W (Fig. 2). These areas correspond to regions of maximum modeled ice deposition during past moderate-to-high obliquity periods, as predicted by the LMD Global Climate Model (GCM) and supported by data from the SWIM (Subsurface Water Ice Mapping) project.

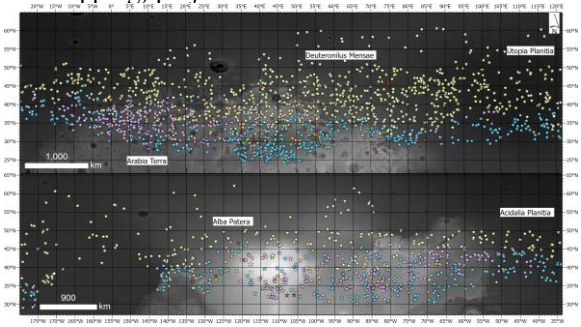

Fig. 2: Spatial distribution of each crater fill type in the northern hemisphere, highlighting areas of concentration.

Regional Climatic Controls: The formation and spatial distribution of crater fill types in the northern mid-latitudes of Mars are consistent with glacial processes during periods of moderate to high obliquity (Madeleine et al., 2006). In this scenario, sublimation of equatorial ice sources increases atmospheric water vapor, while elevated dust levels enhance the atmosphere's ability to retain moisture. This leads to a shift in the vapor saturation zone from the poles to the mid-latitudes. Poleward transport of moisture, driven by strong stationary planetary waves and transient weather systems, results in the condensation and precipitation of ice, forming a thick cloud belt across the northern mid-latitudes. Ice is then deposited in topographic traps such as crater interiors and preserved preferentially on pole-facing slopes due to lower insolation. Our mapping results reflect this climatic control: Type 1 (HDFR) and Type 2 (HDF), which exhibit well-preserved, ice-rich textures, are concentrated between 25°–42°N, corresponding to regions like northern Arabia Terra and Alba Patera, where modeled precipitation is highest. Conversely, Type 5 (DIRF) and Type 6 (PF) are dominant between 35°–50°N, particularly in Deuteronilus–Protonilus Mensae and Utopia Planitia, where accumulation occurs but is offset by intense sublimation and collapse, consistent with model-predicted seasonal ice loss.

Comparison with Subsurface Water Ice on Mars (SWIM): To evaluate the relationship between mapped crater fills and modelled ground ice, we compared our classification results with the SWIM project maps (Fig. 3b–d) (Morgan et al., 2025). Out of 4106 craters analyzed, approximately 52% of Type 1 and 2 fills coincide with zones of ≥60% consistency in the 0–5 m SWIM layer, suggesting a strong spatial correspondence between preserved fill types and modeled shallow ground ice. Regional associations between crater fill types and SWIM ice consistency include the following:

- Acidalia Planitia (30-40°N/-10-30°E): High density of Type 1 fills (HDFR), overlapping with high SWIM consistency zones at all depths.
- Alba Patera (30-40°N/-60-120°W): Frequent Type 2 fills associated with moderately consistent 0–1 m ice stability.
- North of Arabia Terra (30-40°N/0-60°E): Type 2 fills correlate with regions of enhanced winter precipitation (Forget et al., 2009).
- Deuteronilus–Protonilus Mensae (35-60°N/40-80°E): Abundant Type 5 fills coincide with >5 m SWIM consistency zones and degraded ice morphology.
- Utopia Planitia (35-60°N/80-125°E): Mix of Type 5 and 6 fills within low–moderate SWIM zones; region also exhibits polygonal ground.
- Near 25°N (30-60°E): Scattered Type 1 and 2 fills fall near equatorward margins of SWIM's stable ice zone, suggesting rare preservation of shallow ice at lower latitudes.

The mapping revealed that high-definition crater fills are primarily concentrated between 25°–40°N, with dense clustering in three key regions: Arabia Terra (0°–60°E), Utopia Planitia (80°–125°E), and Alba Patera (-60-120°W). All three areas are known for their substantial subsurface ice, making them strong

candidates for future crewed landing sites. Among them, the northern part of Arabia Terra, where Type 1 fills are prominent, stands out as especially promising. The presence of clustered ring-mold craters in this region indicates shallow, ice-rich substrates, making it a compelling target for future exploration missions such as Mars Ice Mapper, which aims to locate accessible subsurface ice for in situ resource utilization in human exploration.

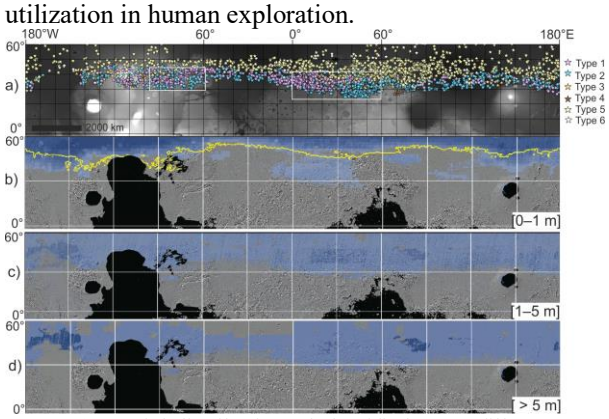

Fig 3: a) Spatial distribution of classified crater fill across the Martian mid-latitudes (25°60° N) b) Subsurface ice consistency map of 0–1 m depth by the SWIM project c) Subsurface ice consistency map of 0–5 m depth by the SWIM project d) Subsurface ice consistency map of >5 m depth by the SWIM project

These regional distributions align with previous findings, including Sako et al. (2025), which document widespread periglacial features (polygons, fractured mounds, and Brain Terrains) indicative of shallow ground ice.

Conclusion: Our classification of over 4000 mid-latitude craters reveals clear spatial trends in the preservation and degradation of ice-rich crater fills, reflecting past climate conditions influenced by obliquity-driven cycles. of fill types from well-preserved HDFR and HDF to degraded DIRF and PF provides a morphological record of episodic ice accumulation, loss, and surface modification. Notably, the equatorward presence of Type 1 and 2 fills near 25°N suggests localized preservation of shallow ground ice beyond predicted latitudinal limits.

These results help refine our understanding of subsurface ice stability thresholds and offer critical spatial constraints for climate modeling on Mars. Future work should integrate crater fill morphologies into obliquity-modulated GCM frameworks and inform landing site selection for missions targeting in-situ ice access and climate reconstruction.

References:[1] Levy J. S., Head J. W., & Marchant D. R. (2009) *Icarus*, 202:462 476. [2] Levy J. S., Head J. W., & Marchant D. R. (2010) *Icarus*, 209:390 404. [3] Levy J. S., Fassett C. I., Head J. W., Schwartz C., & Watters J. L. (2014) *J. Geophys. Res. Planets*, 119:2188 2196. [4] Kress A. M. & Head J. W. (2008) *Geophys. Res. Lett.*, 35: L23206. [5] McEwen A. S., Eliason E. M., Bergstrom J. W., Bridges N. T., Hansen C. J., Delamere W. A., et al. (2007) *J. Geophys. Res. Planets*, **112**(E5). [6] Malin M. C., Bell III J. F., Cantor B. A., Caplinger M. A., Calvin W. M., Clancy R. T., et al. (2007) *J. Geophys. Res. Planets*, **112**(E5). [7] Smith D. E., Zuber M. T., Frey H. V., Garvin J. B., Head J. W., Muhleman D. O., et al. (2001) *J. Geophys. Res. Planets*, **106**(E10):23689–23722. [8] Forget F., Wordsworth R., Millour E., Madeleine J.-B., & Kerber L. (2006) *Science*, 311:368 371. [9] Madeleine J.-B., Forget F., Millour E., & Montmessin F. (2009) *Icarus*, 203:390 405. [10] Morgan G. A., Putzig N. E., Baker D. M., Pathare A., Dundas C. M., Russell M. B., et al. (2025) Planet. Sci. J., 6:29. [10] Sako T., Hasegawa H., Ruj T., Komatsu G., & Sekine Y. (2025) J. Geophys. Res. Planets, 130: e2023JE008232.